Peer-reviewed version available at *Appl. Sci.* **2020**, *10*, 5415; doi:10.3390/app10165415

Article

Facile Synthesis of Highly Conductive Vanadium Doped NiO Film for Transparent Conductive Oxide

Ashique Kotta [1] and Hyung Kee Seo [1,*]

[1] Multifunctional Hybrid Nanomaterials Laboratory, School of Chemical Engineering, Jeonbuk National University, Jeonju 54896, Republic of Korea; kottaash@jbnu.ac.kr

* Correspondence: hkseo@jbnu.ac.kr;

Abstract: Metal oxide based electrodes play a crucial role in various as a transparent conductive oxide (TCO). One of the metal oxides, nickel oxide is a promising electrical conductive material. Here, we display that incorporation of vanadium in NiO lattice significantly improve both electrical conductivity and hole extraction. Also, vanadium doped nickel oxide exhibits a lower crystalline size compared to pristine nickel oxide, which maintains the reduction of surface roughness. These results indicating that the vanadium is an excellent dopant for NiO.

Keywords: vanadium doping; size tuning; bandgap; transparent conductive oxide; electrical conductivity.

1. Introduction

Nickel oxide (NiO) is one of the rare metal oxide semiconductors, exhibiting a wide bandgap of ~ 3.6 eV [1-3]. It has been used in numerous practical applications, such as organic light-emitting diode [4], sensor [5], supercapacitor [6] and solar cells [7]. There are many literature reports available on the synthesis of NiO nanoparticles (NPs) [8-11]. However, they suffer to prepare a well-dispersed ultra-small NiO ink for transparent conductive oxide (TCO) applications [12,13]. In reality, an electrode fabrication using pre-annealed NiO nanoparticles is difficult due to the less dispersibility, and poor adhesion on TCO substrates. Capping agent like oleylamine and oleic acid adding during the synthesis of metal oxide beneficial for the suppression of particle growth and eventually can achieve monodispersed metal oxide nanoparticles with great dispersion on DI water.

From the recent reports, NiO used as hole transport layer (HTL) in inverted perovskite solar cell [14-16] and organic light-emitting diode (LED) [17]. In principle, to enhance the performance of solar cells and OLED needs to overcome following general requirements such as: better electrical conductivity, efficient charge-transporting, solution processing under low temperature and bandgap tuning [18]. To improve the electrical conductivity and hole extraction can be achieved through doping [19]. Different dopants have been used to improve the conductivity of NiO, such as Cs [19], Cu [20], Nb [21], Y [22], Ag [1], Co [23], N [24] and K [25]. Among all these dopants, light Cu doping is widely used in various TCO based applications.

A notable research by Wei Chen et al. [20] had reported that Cu doping on NiO will drastically enhance the electrical conductivity of NiO. More recently, Julien et al. reported that N doped NiO improved the conductivity as compared to undoped NiO by the influence of Ni vacancies [24]. The work of Islam et al. also demonstrated that NiO film with superior conductivity by a higher ratio of Ni^{3+}/Ni^{2+} [26].

In this work, for the first time, to the best of our knowledge, we studied the optical, morphological and electrical conductivity of V:NiO. Our main aim is to investigate that how to modify the NiO film conductivity on the TCO substrate. So we substitute Ni by varying weight percentages of vanadium on NiO lattice. The comparative study of pristine NiO and V:NiO result showed improvement of film morphology and conductivity as compared to pristine NiO film. Both

pristine and V doped NiO were prepared by solvothermal decomposition method. Ultra-small sized highly crystalline pre-annealed nanoparticles were used for the deposition on the TCO substrate. However, effect of vanadium doping on NiO has not been widely studied.

2. Materials and Methods

2.1. Materials and Methods

Materials including Ni (II) acetylacetonate ($C_{10}H_{14}NiO_4$), Oleylamine ($C_{18}H_{37}N$), Borane tri-ethylamine [$(C_2H_5)_3NBH_3$] and vanadium pentoxide (V_2O_5) were purchased from Sigma-Aldrich.

2.2. Characterizations

The properties of both pristine and varying concentrations of vanadium doped NiO (V:NiO) nanoparticles were characterized by the Field emission scanning electron microscopy (FESEM, Hitachi S-4700, Tokyo, Japan), transmission electron microscopy (TEM, JEM-2010-JEOL, Tokyo, Japan), X-Ray diffractometer (XRD, PAN alytical X'Pert PRO, Netherlands), Raman spectroscopy (Renishaw, UK), Ultraviolet-visible spectroscopy (UV-vis, Jasco V-670, Easton, MD, USA) and X-ray photoelectron spectroscopy (XPS, AXIS-NIVA CJ 109, Kratos, Manchester, UK). The film properties were characterized by tapping mode of atomic force microscopy (Bruker, Multimode-8, Massachusetts, USA) and source meter (Keithley-2450, Beaverton, USA).

2.3. Synthesis of pristine and V doped NiO

Nickel oxide (NiO) nanoparticles were synthesized by the solvothermal decomposition method. Briefly, 1 mmol of Ni(II) acetylacetonate was dissolved in 15 ml of oleylamine. The solution was kept in a two necked round flask and heated to 110°C with continuous stirring under nitrogen flow for 45 minutes. The obtained clear blue solution then cooled to and maintained at 90°C. Next, a mixture of 0.4 ml of borane tri-ethylamine and 2 ml oleylamine quickly injected into the clear solution. The resulting dark solution continuously stirred for 1 hrs. The resultant solution containing ultra-small sized NiO nanoparticles were collected by 6000 rpm centrifugation for 15 minutes. Then NPs have washed ethanol by three times. For the Vanadium doped NiO (V:NiO), different weight percentages of vanadium pentoxide were added with Ni(II) acetylacetonate and oleylamine solution. Followed all other conditions similar to the synthesis of the pristine NiO. In this reaction oleylamine acts as a capping agent, which helps to reduce particle growth and borane tri-ethylamine used as a reducing agent, as shown in scheme 1. As synthesized pristine NiO and V: NiO were easily dispersed in DI water by 30 minutes ultra-sonication. Pristine and doped NiO films were deposited under room temperature on cleaned FTO glass substrates by spin coating (2500 rpm, 60 s) with the solutions which was mentioned above.

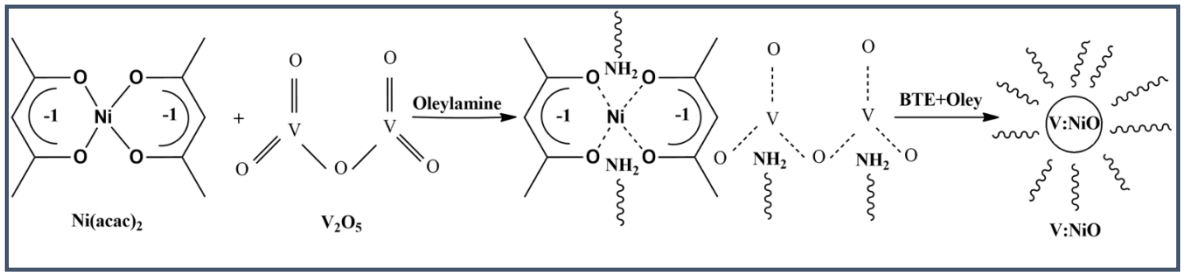

Scheme 1. Synthesis of V:NiO nanoparticles by solvothermal decomposition of V:Ni-oleylamine complex.

3. Results

3.1. Study of material properties

To study the effect of V-doping on NiO, the materials were subjected to analysis using XRD. In our work, both pristine and doped NiO NPs exhibited a very broad XRD pattern (Figure 1(a)). The diffraction peaks of prepared powder samples shows the cubic face-centered crystal system with four characteristic diffraction peaks at 2θ = 36.98°, 43.21°, 62.67°, and 75.34°, which could be assigned to the (111), (200), (220) and (311) planes of NiO, respectively. The synthesized NiO NPs formation confirmed from the joint committee on powder diffraction standard (JCPDS) card no. 03-065-2901 with the space group of Fm3m [27]. Meanwhile, no extra diffraction peaks related to vanadium or vanadium oxide were observed. This result indicates that the light doping concentration of V could hardly change the phase structure of NiO [1]. Additionally, it could be observed that the V:NiO NPs diffraction peak at 43.251° shows a broadening and slight shifting towards a higher angle (Figure 1(b)). This result is indicating the incorporation of vanadium in NiO lattice. Also important to mention that the diffraction peak broadening of V:NiO sample leads to the reduction of particle size. To understand the effect of particles size after doping, further, we calculated the crystalline size of both samples by Debye-Scherrer formula, $D_p = \frac{0.89\,\lambda}{\beta cos\theta}$. Where D_p is the crystalline size, λ is the x-ray wavelength, β is the full width half maximum (FWHM) and θ is the diffraction angle of the peak. Interestingly, we observed the crystalline size of peak (200) significantly decreased after doping from 3.09 nm to 2.82 nm. Hence, the dissociation density (δ) and lattice strain (ε) were calculated by equation [28], $\delta = {1}/{D_p{}^2}$ and $\varepsilon = \beta cos\theta/4$ and values are tabulated in Table 1. It can be concluded that NiO crystalline size decreased by V doping, thereby, dissociation density and lattice strain enhanced.

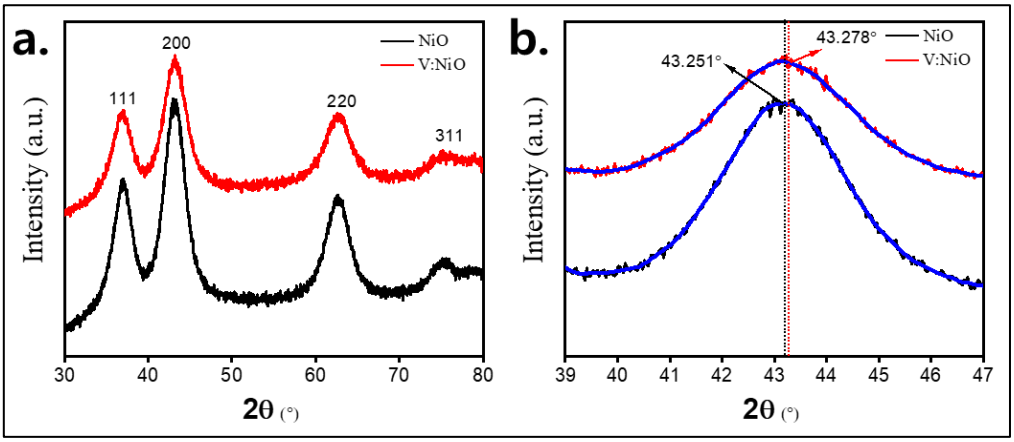

Figure 1. (a) XRD spectra of pristine and V:NiO NPs and (b) enlarged XRD spectra of pristine NiO and V:NiO NPs.

Table 1. Measured values of structural parameters for NiO and V:NiO

Samples	2θ (°)	hkl	FWHM	d_{sp} (A°)	D_p (nm)	δ (nm^{-1})	ε×10^{-2}
NiO	43.251	200	2.94	2.095	3.04	0.1082	0.955
V:NiO	43.278	200	3.17	2.094	2.82	0.1257	1.054

Figure 2(a) shows that the FT-IR spectra of $Ni(ac)_2$, V_2O_5, NiO and V:NiO for the comparative studies of precursor materials and products. In our case, the characteristic stretching vibration of Ni-O absorption band was observed at 468 cm^{-1} which is originated from the $Ni(ac)_2$ species. The peak at 676 cm^{-1} in the doped sample ascribed the presence of vanadium.

Preprints (www.preprints.org) | NOT PEER-REVIEWED | Posted: 5 July 2020 doi:10.20944/preprints202007.0069.v1

Peer-reviewed version available at Appl. Sci. 2020, 10, 5415; doi:10.3390/app10165415

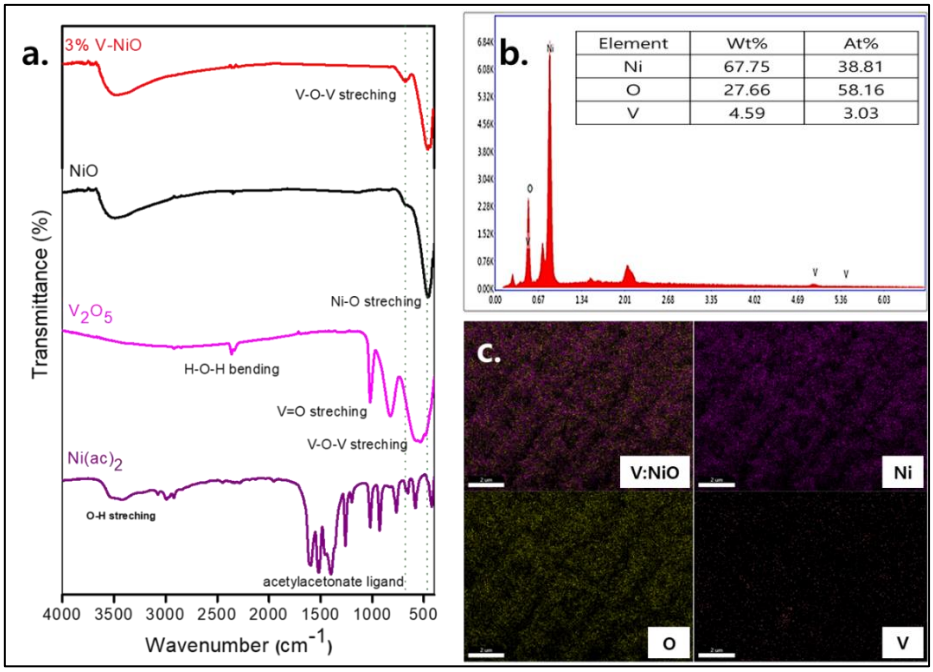

Figure 2. (a) FTIR spectra of NiO and V:NiO with precursor materials, (b) EDS spectra of V:NiO NPs and (c) EDS elemental mapping of the corresponding elements of Ni, O and V (scale bar-2μm).

The elemental composition of both pristine and V:NiO NPs confirmed by energy-dispersive x-ray spectroscopy (EDAX). Figure 2(b) shows that V:NiO powder sample exist of Ni, V, and O with no impurity elements. The weight and atomic percentage values of Ni, O and V elements are given in the inset of Figure 2(b). The EDX mapping of elements in Figure 2(c) revealed the uniform distribution of Ni, V, and O in the sample.

Raman spectra of NiO and V:NiO were given in Figure 3(a). From the analysis, four characteristic Raman peaks are positioned in both samples, which are corresponding to the shaking peaks of NiO. The peaks at 324, and 479 cm^{-1} are first-order transverse optical (TO) and longitudinal optical (LO) phonon modes of NiO NPs, respectively. The peaks at 546 and 686 cm^{-1} are because of the combination of 2TO and 2LO. Meanwhile, an extra peak observed at 760 cm^{-1} can be associated with the V-O stretching mode in V:NiO sample. This result shows that vanadium can be incorporated with oxygen.

Figure 3(b-c) depicts the ultraviolet-visible spectroscopy studies of ethanol dispersed pristine and doped NiO samples. A gradual red shift in absorption spectra with increasing V concentration is observed from Figure 3b. The shift is consistent with the incorporation of V^{5+} into the NiO lattice. This indicates that the band gap energy in V:NiO is lower than that of pristine NiO. Meanwhile, the optical band gap estimated for pristine NiO NPs by Tauc plot (Figure 3(c)) revealed around 3.65 eV, which is well-matched with the previously reported values [3, 2]. In the case of V-NiO NPs, it was clear that after introducing vanadium content in NiO crystal lattice, the optical band gap slightly gets reduced into 3.62 eV for 1.5% V:NiO and 3.59 eV for 3% V:NiO.

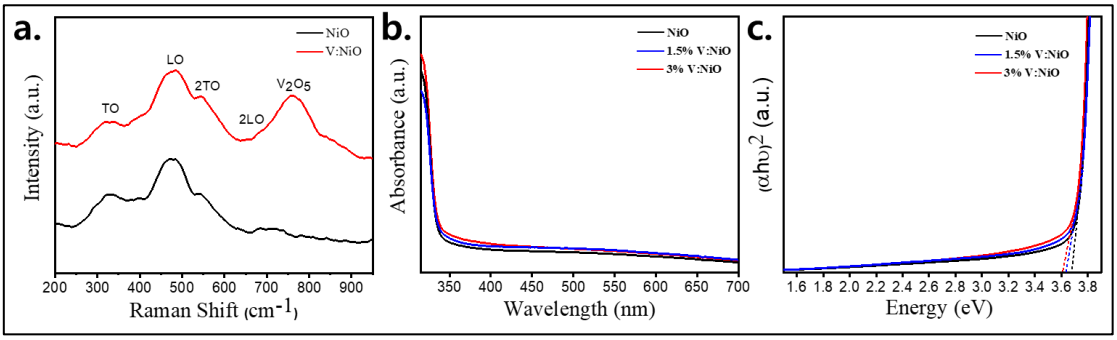

Figure 3. (a) Raman spectra of NiO and V:NiO NPs powder samples, (c) UV-absorption spectra of diluted NiO and V:NiO NPs solution and (c) Corresponding Tauc plots of the absorption spectra.

The FE-SEM micrograph images with higher resolution images of pristine NiO and V:NiO powder samples are shown in Figure 4(a-b). Both samples exhibit similar morphology with ultra-small sized spherical structures that are agglomerated. The TEM image with the same morphology of the samples displayed in Figure 4(c-d). The particle diameters are summarized in Figure 4(e). The statistical distributions of nanoparticles diameter of pristine NiO and V:NiO measured to be ~3.5±0.5 nm and ~2.5±0.5 nm, respectively. The result was consistent with the result of XRD. The particle size variations in the TEM analysis of both samples may influence of large Ni ions (ionic radius- 0.83 A°) replaced by the small V ion (ionic radius- 0.72 A°). Meanwhile, the HR-TEM results reveals that the incorporation of V into the NiO lattice slightly reduced the interplanar distance (inset images) from 0.2095 nm to 0.2094 nm.

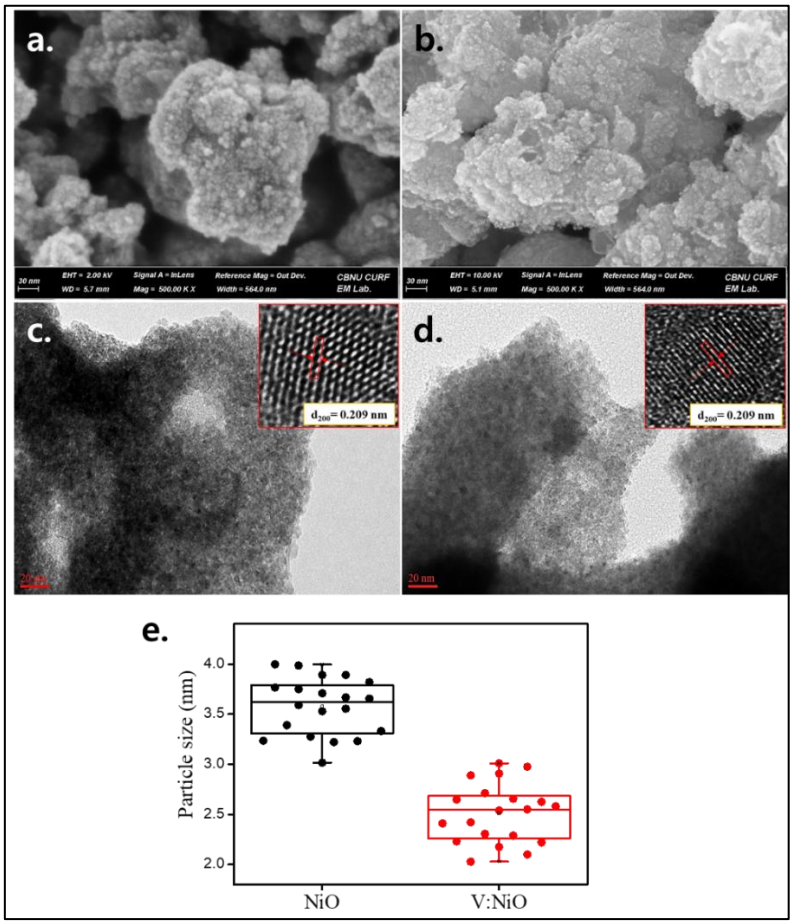

Figure 4. (a) FE-SEM images of (a) NiO and (b) V:NiO and TEM patterns of (a) NiO (inset: HR-TEM image of NiO) and (b) V:NiO (inset: HR-TEM image of V:NiO)) and (e) statistics of particles distribution of NiO and V:NiO samples.

Elemental analysis was characterized by X-ray photoelectron spectroscopy. The survey spectra of pristine NiO (Figure 5(a)) confirmed that the presence of Ni and O elements, whereas Ni, O and V elements in V:NiO sample (Figure 5(d)). Typically NiO $2P_{3/2}$ consists of the main peak at 854 eV, shoulder peak at 856 eV and shake up satellite peak at 861 eV [29]. No major changes observed in a comparison of Ni $2P_{3/2}$ spectra of both pristine and doped samples (Figure 5(b and e)). But in the case of doped sample detected the presence of V^{4+} and V^{5+} in the binding energy range between 526 eV to 510 eV, which reveals that V atom had been successfully incorporated into NiO crystal lattice. Interestingly, after V occupied the interstitial sites in the NiO lattice, possibly the Ni^{3+} ions induced by V^{5+} ions (Figure 5(e)). Further, we calculated the ratio between Ni^{3+}/Ni^{2+} and it was calculated to be 0.96 and 1.04 for NiO and V:NiO samples, respectively. The higher density of Ni^{3+} state in V:NiO crystal would contribute to the improvement of p-type conductivity [29].

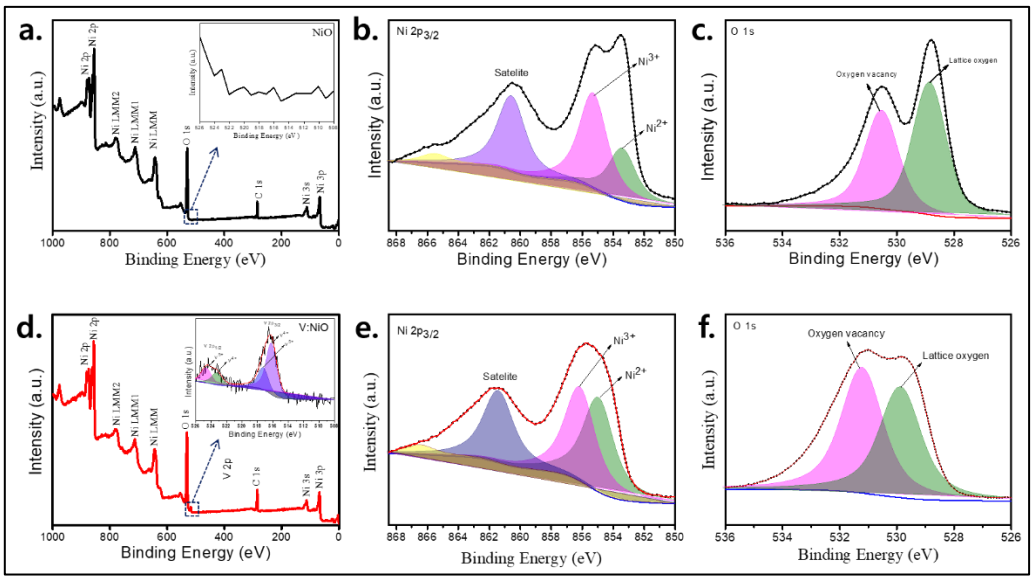

Figure 5. (a-c) XPS spectra of NiO: (a) survey spectra (inset: high resolution spectra of V 2p), high resolution (b) Ni $2p_{3/2}$, (c) O 1s and (d-e) XPS spectra of V:NiO: (a) survey spectra (inset: high resolution spectra of V 2p), high resolution (b) Ni $2p_{3/2}$, (c) O 1s.

3.2. Study of film properties

The morphology of the surface of the thin films of pristine NiO and V:NiO were studied using the atomic force microscopy. Figure 6 (a-d) shows that the AFM topography and three dimensional (3D) images of NiO and V:NiO on the FTO substrate. After doping the clear observation of particle size reduction were also confirmed from AFM topographic images. Both films showing a closely packed uniform morphology and exhibit root mean square (RMS) surface roughness at 2.94 nm and 2.49 nm for the pristine NiO and V:NiO films, respectively. The reduction of surface roughness values in film after doping, indicating that a small amount of vanadium in the NiO lattice will be beneficial for the various transparent conductive oxide applications [1,20,22,17].

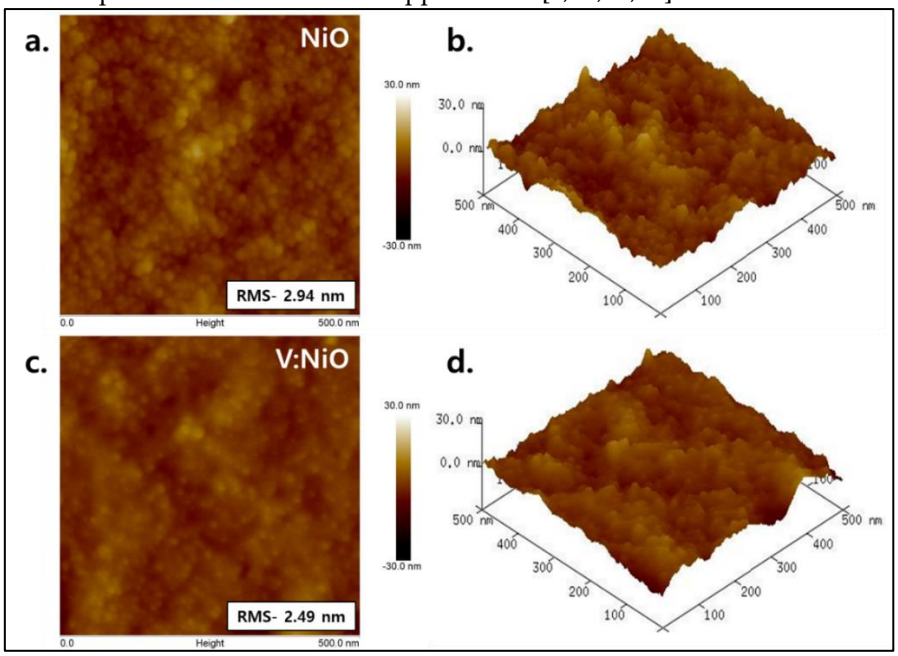

Figure 6. AFM topography and 3D AFM images of (a-b) NiO NPs and (c-d) V:NiO.

We investigated the influence of V doping on the electrical conductivity of the NiO thin films obtained by the photovoltaic measurement system. For that, we fabricated FTO/NiO or V:NiO/Ag

film and measured the current-voltage (I-V) curve. The following equation calculated the conductivity of the films.

$$\sigma = \frac{d}{A \times R}$$

Where σ is the conductivity, d is the thickness of the films, A is the active area and R is the resistance obtained from the I-V curve. As shown in the Figure 7, replacing the pristine NiO film with a V:NiO film significantly increased the vertical current, which indicating the enhancement of electrical conductivity upon V doping. The conductivity of pristine NiO and V:NiO films were estimated to be 2.9×10^{-6} Scm^{-1} and 3.9×10^{-6} Scm^{-1}, respectively. The enhancing conductivity of V:NiO compared to pristine NiO film about 34.4%, due to the enrich of Ni^{3+} ion in V:NiO sample [23]. This point extensively discussed in XPS analysis. Definitely, this result demonstrate that V-doping can be a powerful way to control the electrical conductivity of NiO.

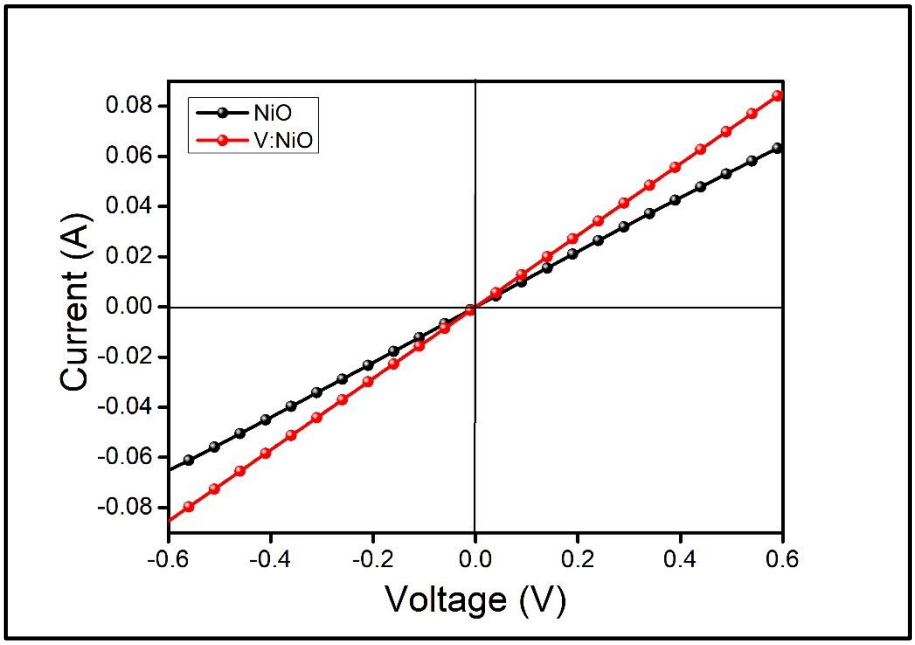

Figure 7. I-V curve of NiO and V:NiO films based on the structure of FTO/NiO or V:NiO/Ag; the inset show corresponding fabricated electrode structure.

4. Conclusion

In conclusion, pristine NiO and vanadium (V) doped NiO were successfully synthesized by a solvothermal decomposition method and deposited on the FTO substrate. The V doped NiO (V:NiO) film exhibits a lower crystalline size compared to pristine NiO film. A systematic analysis of crystallographic, optical and morphological investigation showed that the V content in NiO lattice would be beneficial for optoelectronic device applications. Also, the AFM investigations of the V:NiO display that the root mean square (RMS) surface roughness lowered in comparison to the pristine NiO film. Finally, I-V curve shows that the conductivity of V:NiO film effectively enhanced about 34.4%. The improvement of electrical conductivity can promote better charge transport and reduction of interfacial charge accumulation.

Author Contributions: A.Kotta performed the experiments and wrote the manuscript. H.K.Seo. contributed to the preparation and revision of the manuscript.

Funding: This work was supported by a National Research Foundation of Korea (NRF) Project #2018 R1A4A102552813.

Conflicts of Interest: The authors declare no conflict of interest.

References

1. Zheng, J.; Hu, L.; Yun, J.S.; Zhang, M.; Lau, C.F.J.; Bing, J.; Deng, X.; Ma, Q.; Cho, Y.; Fu, W.; et al. Solution-Processed, Silver-Doped NiO x as Hole Transporting Layer for High-Efficiency Inverted Perovskite Solar Cells. *ACS Appl. Energy Mater*. 2018, 1, 561–570.
2. Hu, L.; Peng, J.; Wang, W.; Xia, Z.; Yuan, J.; Lu, J.; Huang, X.; Ma, W.; Song, H.; Chen, W.; et al. Sequential Deposition of CH3NH3PbI3 on Planar NiO Film for Efficient Planar Perovskite Solar Cells. *ACS Photonics* 2014.
3. Zhai, Z.; Huang, X.; Xu, M.; Yuan, J.; Peng, J.; Ma, W. Greatly Reduced Processing Temperature for a Solution-Processed NiO x Buffer Layer in Polymer Solar Cells. *Adv. Energy Mater*. 2013, 3, 1614–1622.
4. Im, H.C.; Choo, D.C.; Kim, T.W.; Kim, J.H.; Seo, J.H.; Kim, Y.K. Highly efficient organic light-emitting diodes fabricated utilizing nickel-oxide buffer layers between the anodes and the hole transport layers. *Thin Solid Films* 2007.
5. Amin, S.; Tahira, A.; Solangi, A.; Mazzaro, R.; Ibupoto, Z.H.; Vomiero, A. A sensitive enzyme-free lactic acid sensor based on NiO nanoparticles for practical applications. *Anal. Methods* 2019, 11, 3578–3583.
6. Vijayakumar, S.; Nagamuthu, S.; Muralidharan, G. Supercapacitor studies on NiO nanoflakes synthesized through a microwave route. *ACS Appl. Mater. Interfaces* 2013, 5, 2188–2196.
7. Seo, S.; Park, I.J.; Kim, M.; Lee, S.; Bae, C.; Jung, H.S.; Park, N.G.; Kim, J.Y.; Shin, H. An ultra-thin, un-doped NiO hole transporting layer of highly efficient (16.4%) organic-inorganic hybrid perovskite solar cells. *Nanoscale* 2016, 8, 11403–11412.
8. Natarajan, C.; Matsumoto, H.; Nogami, G. Improvement in electrochromic stability of electrodeposited nickel hydroxide thin film. *J. Electrochem. Soc*. 1997.
9. Song, X.; Gao, L. Facile synthesis of polycrystalline NiO nanorods assisted by microwave heating. *J. Am. Ceram. Soc*. 2008, 91, 3465–3468.
10. Šurca, A.; Orel, B.; Pihlar, B.; Bukovec, P. Optical, spectroelectrochemical and structural properties of sol-gel derived Ni-oxide electrochromic film. *J. Electroanal. Chem*. 1996, 408, 83–100.
11. Wang, W.N.; Itoh, Y.; Lenggoro, I.W.; Okuyama, K. Nickel and nickel oxide nanoparticles prepared from nickel nitrate hexahydrate by a low pressure spray pyrolysis. Mater. Sci. Eng. B *Solid-State Mater. Adv. Technol*. 2004, 111, 69–76.
12. Qiu, Z.; Gong, H.; Zheng, G.; Yuan, S.; Zhang, H.; Zhu, X.; Zhou, H.; Cao, B. Enhanced physical properties of pulsed laser deposited NiO films via annealing and lithium doping for improving perovskite solar cell efficiency. *J. Mater. Chem. C* 2017, 5, 7084–7094.
13. Bai, Y.; Chen, H.; Xiao, S.; Xue, Q.; Zhang, T.; Zhu, Z.; Li, Q.; Hu, C.; Yang, Y.; Hu, Z.; et al. Effects of a Molecular Monolayer Modification of NiO Nanocrystal Layer Surfaces on Perovskite Crystallization and Interface Contact toward Faster Hole Extraction and Higher Photovoltaic Performance. *Adv. Funct. Mater*. 2016, 26, 2950–2958.
14. Sun, J.; Lu, J.; Li, B.; Jiang, L.; Chesman, A.S.R.; Scully, A.D.; Gengenbach, T.R.; Cheng, Y.B.; Jasieniak, J.J. Inverted perovskite solar cells with high fill-factors featuring chemical bath deposited mesoporous NiO hole transporting layers. *Nano Energy* 2018, 49, 163–171.
15. Zhang, H.; Cheng, J.; Lin, F.; He, H.; Mao, J.; Wong, K.S.; Jen, A.K.Y.; Choy, W.C.H. Pinhole-free and surface-nanostructured niox film by room-Temperature solution process for high-performance flexible perovskite solar cells with good stability and reproducibility. *ACS Nano* 2016, 10, 1503–1511.
16. Yin, X.; Chen, P.; Que, M.; Xing, Y.; Que, W.; Niu, C.; Shao, J. Highly Efficient Flexible Perovskite Solar Cells Using Solution-Derived NiOx Hole Contacts. *ACS Nano* 2016, 10, 3630–3636.
17. Liu, S.; Liu, R.; Chen, Y.; Ho, S.; Kim, J.H.; So, F. Nickel oxide hole injection/transport layers for efficient solution-processed organic light-emitting diodes. *Chem. Mater*. 2014, 26, 4528–4534.
18. He, Q.; Yao, K.; Wang, X.; Xia, X.; Leng, S.; Li, F. Room-Temperature and Solution-Processable Cu-Doped Nickel Oxide Nanoparticles for Efficient Hole-Transport Layers of Flexible Large-Area Perovskite Solar Cells. *ACS Appl. Mater. Interfaces* 2017, 9, 41887–41897.
19. Chen, W.; Liu, F.-Z.; Feng, X.-Y.; Djurišić, A.B.; Chan, W.K.; He, Z.-B. Cesium Doped NiO x as an Efficient Hole Extraction Layer for Inverted Planar Perovskite Solar Cells. *Adv. Energy Mater*. 2017, 7, 1700722.
20. Jung, J.W.; Chueh, C.C.; Jen, A.K.Y. A Low-Temperature, Solution-Processable, Cu-Doped Nickel Oxide Hole-Transporting Layer via the Combustion Method for High-Performance Thin-Film Perovskite Solar Cells. *Adv. Mater*. 2015, 27, 7874–7880.
21. Sun, X.; Li, B.; Metiu, H. Ethane activation by Nb-doped NiO. *J. Phys. Chem*. C 2013, 117, 23597–23608.

22. Hu, Z.; Chen, D.; Yang, P.; Yang, L.; Qin, L.; Huang, Y.; Zhao, X. Sol-gel-processed yttrium-doped NiO as hole transport layer in inverted perovskite solar cells for enhanced performance. *Appl. Surf. Sci*. 2018, 441, 258–264.
23. Xie, Y.; Lu, K.; Duan, J.; Jiang, Y.; Hu, L.; Liu, T.; Zhou, Y.; Hu, B. Enhancing Photovoltaic Performance of Inverted Planar Perovskite Solar Cells by Cobalt-Doped Nickel Oxide Hole Transport Layer. *ACS Appl. Mater. Interfaces* 2018, 10, 14153–14159.
24. Keraudy, J.; Ferrec, A.; Richard-Plouet, M.; Hamon, J.; Goullet, A.; Jouan, P.Y. Nitrogen doping on NiO by reactive magnetron sputtering: A new pathway to dynamically tune the optical and electrical properties. *Appl. Surf. Sci*. 2017, 409, 77–84.
25. Chen, P.C.; Yang, S.H. Potassium-Doped Nickel Oxide as the Hole Transport Layer for Efficient and Stable Inverted Perovskite Solar Cells. *ACS Appl. Energy Mater*. 2019, 2, 6705–6713.
26. Islam, M.B.; Yanagida, M.; Shirai, Y.; Nabetani, Y.; Miyano, K. NiO x Hole Transport Layer for Perovskite Solar Cells with Improved Stability and Reproducibility. *ACS Omega* 2017, 2, 2291–2299.
27. Kwon, U.; Kim, B.-G.; Nguyen, D.C.; Park, J.-H.; Ha, N.Y.; Kim, S.-J.; Ko, S.H.; Lee, S.; Lee, D.; Park, H.J. Solution-Processible Crystalline NiO Nanoparticles for High-Performance Planar Perovskite Photovoltaic Cells. *Sci. Rep*. 2016, 6, 30759.
28. AlFaify, S.; Shkir, M. A facile one pot synthesis of novel pure and Cd doped PbI2 nanostructures for electro-optic and radiation detection applications. *Opt. Mater. (Amst)*. 2019, 88, 417–423.
29. Geng, X.; Lahem, D.; Zhang, C.; Li, C.-J.; Olivier, M.-G.; Debliquy, M. Visible light enhanced black NiO sensors for ppb-level NO2 detection at room temperature. *Ceram. Int*. 2019, 45, 4253–4261.